COLLECTOR AND SOURCE SHEATHS OF A FINITE ION TEMPERATURE PLASMA

by

L. A. Schwager and C. K. Birdsall

Memorandum No. UCB/ERL M88/23

13 April 1988

COLLECTOR AND SOURCE SHEATHS OF A FINITE ION TEMPERATURE PLASMA

by

L. A. Schwager and C. K. Birdsall

Memorandum No. UCB/ERL M88/23

13 April 1988

ELECTRONICS RESEARCH LABORATORY

College of Engineering
University of California, Berkeley
94720

COLLECTOR AND SOURCE SHEATHS OF A FINITE ION TEMPERATURE PLASMA

by

L. A. Schwager and C. K. Birdsall

Memorandum No. UCB/ERL M88/23

13 April 1988

ELECTRONICS RESEARCH LABORATORY

College of Engineering
University of California, Berkeley
94720

Table of Contents

1

Collector and Source Sheaths of a Finite Ion Temperature Plasma

The region between a Maxwellian plasma source and an absorbing surface is modeled with an electrostatic particle simulation and with a kinetic plasma-sheath model. In the kinetic model, Poisson's equation and Vlasov equations govern the velocity distribution of the ions and electrons. Our numerical and theoretical results for collector potential and plasma transport agree with the bounded model of Emmert et al. but differ somewhat from those using traditional Bohm sheath analysis. The plasma source injects equal fluxes of half-Maxwellian ions and electrons with specified mass and temperature ratios and is assumed to have a zero electric field. Representing the potential change within a distributed full-Maxwellian source region, the source potential drop depends primarily on temperature ratio and evolves a few Debye lengths from the source to neutralize the injected plasma. The plasma flows to an electrically floating collector where the more familiar electron-repelling collector sheath appears. Profiles of potential, density, drift velocity, temperature, kinetic energy flux, and heat flux are shown from simulation; all compare very well with theory.

I. INTRODUCTION

A. Problem description

The sheath region between a plasma and a collector is rich in kinetic behavior, having non-Maxwellian velocity distributions of the ions and electrons resulting from large potentials. Time-dependent computer simulations using particles are a prime tool for examining these non-neutral plasma regions and following the dynamics of the plasma-sheath-surface interaction. These simulations provide insight for verifying and improving the kinetic model for the steady state conditions. Consequently we develop both kinetic theory and simulation to analyze the plasma-sheath region and find excellent agreement.

Our numerical and theoretical description is intended to model a bounded plasma with a source generated spatially (not at an emissive surface). The sheath formed near the boundary is collisionless. The plasma flow is normal to the surface and is governed primarily by the self-consistent, internal electrostatic field. This field affects the transport of ions and electrons and their intrinsic energies from the plasma source to the collector. Consequently, the heat load on the collector surface and surface phenomena such secondary electron emission, ion reflection, and sputtering are also dependent on the self-consistent potential. This study is undertaken to describe the strength of the potential which evolves near exposed surfaces of a thermonuclear fusion plasma and within the plasma source itself. In particular, this model may apply to the collisionless plasma flowing to a first wall limiter or diverted to a collector surface. Our analysis applies generally to the end walls or exposed surfaces of any plasma device which fits the above description.

The electrostatic potential ϕ varies gradually over the entire region where Maxwellian ions and electrons are generated at the same rate. This slow variation is observed experimentally by Tonks and Langmuir[1] and is shown analytically by

Emmert *et al.*[2] In the region near the collector, a larger potential change occurs over a distance comparable to the plasma Debye length. These two regions are shown at the top of Fig. 1. The central source region is characterized by a potential change of ϕ_P from its center to the edge of the source region. With the collector potential at ϕ_C, the potential change across the collector sheath is $\phi_C - \phi_P$. The width of the collector sheath is usually many orders of magnitude smaller than the width of the source region. We model this long, distributed source region as a planar source at $x = 0$. Consequently, the slowly varying change in potential to ϕ_P occurs over only a few Debye lengths, as shown in the middle sketch of Fig. 1. Emmert *et al.* have shown that the width of the plasma source does not affect this potential change through the source region. Thus we refer to a "source sheath" which actually represents the gradual potential change over the entire Maxwellian source region.

The boundary conditions imposed on the model for both theory and simulation are as follows. Refer to the bottom of Fig. 1. The plasma source injects steady and equal fluxes of ions and electrons each with half-Maxwellian velocity distributions toward the collector. The temperature and mass ratios of the injected ions and electrons are specified. These particles then flow to the collector surface which becomes charged by the incident particles and floats electrically to ϕ_C.

Electrons, which may be repelled by the internal electrostatic field, return to the plasma source where they are added to the steady flux and also injected at the electron source temperature. Illustrated at the bottom of Fig. 1, this "refluxing" prevents any charge accumulation at the source plane and enforces a zero electric field at the plasma boundary. Hence at the source plane, we distinguish between the injected flux and the emitted flux (injected plus refluxed particles). The net flux (over positive and negative velocities) equals the value of the injected flux. Consequently at steady state, the magnitude of the velocity distribution of emitted

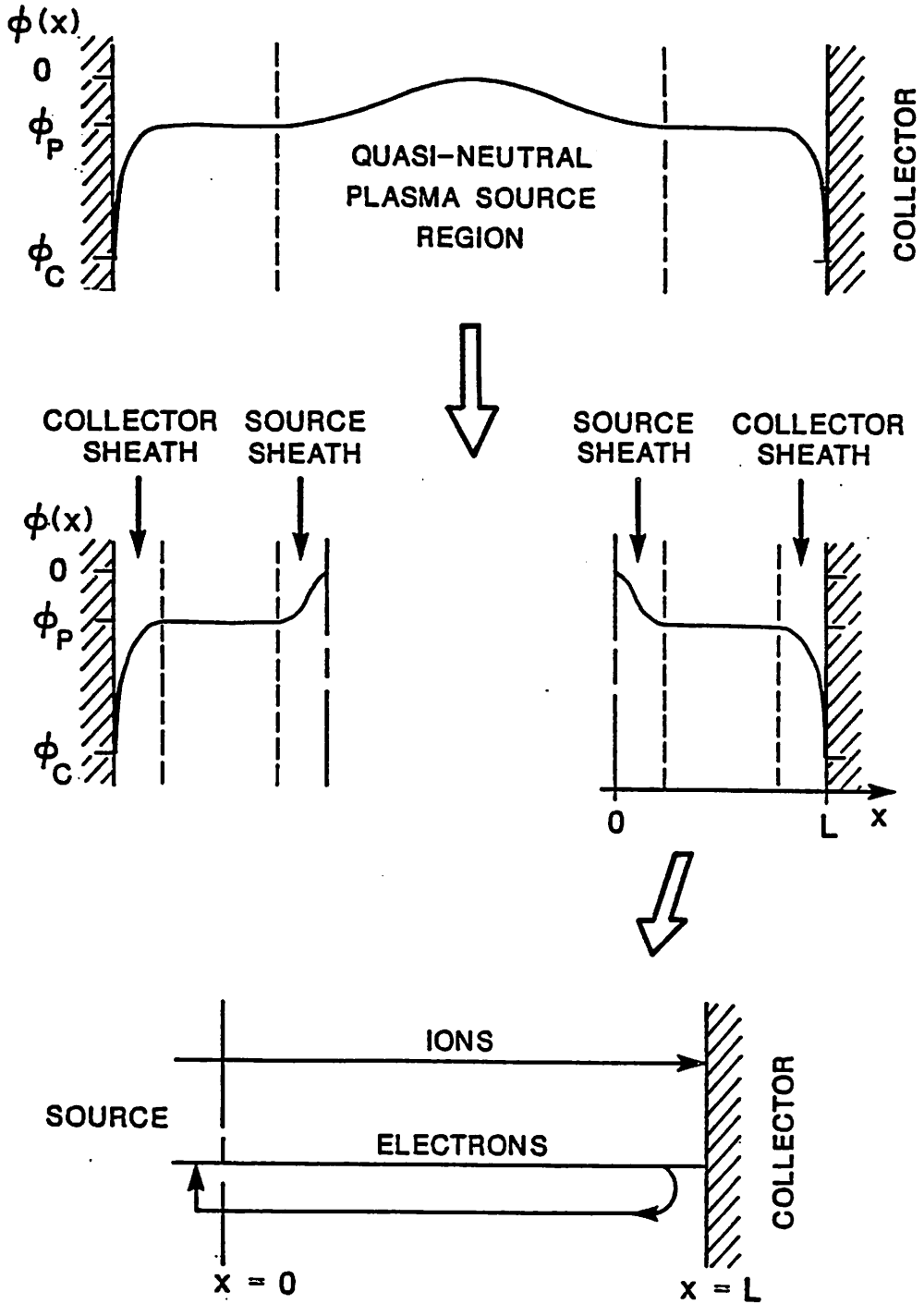

FIG. 1. Model and form of the electrostatic potential profile for the non-Maxwellian sheath region between a Maxwellian plasma source and an electrically floating collector. The top figure indicates the form of the potential profile for a distributed source. The source region is many orders of magnitude longer than the collector sheath region. The middle shows the assumed potential profile for a planar source. The bottom diagrams the flow of particles between the source plane and collector.

electrons increases self-consistently with ϕ_C. The zero field boundary condition with refluxing is similar to that required for a plasma source which drives an ion propulsion system for space travel.[3] In a one-dimensional simulation of this engine, excess electrons are required to be supplied by the source to cause the ions to travel in straight lines away from the source.

The large potential drops near the source and collector, sketched in the middle of Fig. 1, are formed in the following way. With half-Maxwellian sources of equal fluxes of ions and electrons having comparable temperatures and disparate masses, the net plasma charge density is not zero at the source. Consequently a potential drop occurs which returns some electrons to the source and reduces the net electron drift. The source sheath evolves which serves to neutralize the emitted plasma within a few Debye lengths. Thus beyond the source sheath in the neutral region, ion and electron densities equate. However, in this neutral region, both species have non-Maxwellian velocity distributions because of the potential drop from the source. At the floating collector, electrons initially charge the surface and a second electron-repelling sheath evolves which is the traditional collector sheath. Hence, non-neutral source and collector sheaths with a central, neutral region are expected; all are observed numerically and predicted theoretically.

Our bounded, electrostatic particle simulation utilizes the particle-in-cell method for one dimension in space x and velocity v. The time-evolution of the initially empty system is monitored until a steady-state configuration is observed. The transient response and plasma oscillations of the collective behavior are measured. Because the simulation provides the velocity distribution of the ions and electrons in time and space, profiles and histories of various energy and particle fluxes are calculated.

The steady state configuration of the region is analyzed with a plasma-sheath

equation. The full kinetic description of both ions and electrons determines the exact dependence of density on the potential profile. The boundary conditions of zero electric field at the source and zero total current at the collector are applied as above. The electric field is assumed to be zero at the inflection point in potential which occurs in the central region separating the source and collector sheaths by many Debye lengths. With Poisson's equation and the above assumptions and conditions, the values of potential at the neutral region (inflection point) and at the collector are calculated as a function of mass and temperature ratios. With the full kinetic description, various energy and particle fluxes are derived as a function of potential at any spatial location. Details of the above kinetic analysis are provided later in Sec. II. The numerical simulation model and results are presented in Sec. III. A comparison of our theretical and simulation results will be discussed in Sec. IV. The difference between our kinetic model and previous sheath studies which are summarized below is detailed in Sec. V. Conclusions are in Sec. VI.

B. Historical review

In 1929 Tonks and Langmuir[1] developed a model of the plasma-sheath region for a cold ion, warm electron plasma source. Using Poisson's equation, they tied the plasma solution, $\nabla^2\phi \approx 0$, for a distributed source up to the collector, to the plasma-sheath solution which conserves flux in the collisionless, thin sheath. Their plasma equation is solved with a series solution.

Twenty years later Bohm[4] described the evolution of a stable, static potential profile for a plasma of cold ions and warm electrons. Bohm found that, prior to entering the sheath region, the cold ions must acquire a kinetic energy $M\langle V_i^2\rangle/2$ of at least $0.5\,T_{Se}$, where M is the ion mass, $\langle V_i^2\rangle$ is the second velocity moment, and T_{Se} is the electron source temperature (measured in energy units). (Hereafter we use $\langle y\rangle$ to denote the velocity average of the quantity y over all velocities in

the direction normal to the collector surface.) Bohm ascribed this acceleration to small forces evolving over long distances in the plasma outside of the sheath region. Subsequently many similar papers have been written on the stability of the sheath in terms of the ion velocity required to generate the monotonically decreasing potential profile required by the Bohm theory.

Harrison and Thompson[5] solved analytically the model of Tonks and Langmuir ten years after Bohm. A stable sheath criterion is evaluated which is dependent on the moment $\langle V_i^{-2} \rangle$ of ions entering the collector sheath region. This generalized Bohm criterion applies to any velocity distribution of the ions entering the sheath, rather than to only the monoenergetic distribution as assumed by Bohm. However, it is most important to note that they assume the ions have a negligible thermal spread at their source.

A few years later Hall[6] discussed the restrictions of the analysis of Harrison and Thompson to the arbitrary velocity distribution of ions entering the sheath. Hall claims that their results are valid only when few low velocity ions exist at the sheath edge; this allows a stable sheath to evolve, so that, for almost all situations, $\langle V_i^{-2} \rangle^{-1}$ will be nearly equal to $\langle V_i^2 \rangle$. Because the small potential drop caused by the plasma field outside the sheath region, as described by Bohm, is large compared with ion energies, low energy ions do not appear at the sheath edge. Hall concludes that Bohm's simpler model should then be used because nothing qualitative is gained in using the generalized Bohm criterion of Harrison and Thompson.

Recently Stangeby[7] has applied the generalized Bohm criterion to warm source ions. The ion distribution entering the sheath is approximated as a drifting Maxwellian with source temperature T_{Si} (measured in energy units). Treating the sheath edge as a Mach-1 surface, Stangeby assumes isothermal flow so that the incident

ions enter with drift velocity C_S, where

$$C_S = [(T_{Si} + T_{Se})/M]^{1/2},$$

at the same point where ion and electron densities are equal.

Using particle simulation of ions and electrons entering the sheath region, Chodura[8] derives the collector potential by varying the drift velocity V_0 of Maxwellian ions until formation of a potential profile which is not oscillating in space. In a second paper, Chodura[9] uses these values of collector potential for $T_{Si} \ll T_{Se}$ and $T_{Si} = T_{Se}$ to derive the mean ion energy at the collector. Hence ions with an assumed adiabatic flow (specific heat ratio for ions of 5/3) enter the sheath region with $V_0 = C_S$ where

$$C_S = \left(\frac{5}{3}T_{Si} + T_{Se}\right)^{1/2} M^{-1/2}.$$

Unlike the authors following Bohm, Emmert *et al.*[2] have extended the symmetric discharge analysis of Tonks and Langmuir to include the effect of warm ions in the plasma source without assuming that the ions have a particular drift velocity. They tie the solution to the plasma equation for a plasma source with finite ion temperature to the plasma-sheath equation in an infinitely thin sheath. The effect of a warm source which is distributed over a region less than the system length is analyzed. Most interesting is that they observe a flat potential in the sourceless region.

More recently Bissell and Johnson[10] have solved the plasma equation for warm ions but have used the generalized Bohm criterion as a boundary condition. Their analysis produces an infinite electric field at the sheath edge, which compares well with fluid theory but not with the kinetic theory of Emmert *et al*[2]. All of the above

studies, except that of Chodura[8,9], assume electron densities related to potential by a Boltzmann factor.

In a different approach with a more global model, Kuhn[11] studies the axially symmetric, single-ended Q-machine. An emitting plate generates a half-Maxwellian source of plasma with equal ion and electron temperatures. Kuhn varies the ratio of emitted densities at the plate and varies the potential bias applied across the system. A fully kinetic model describes the ions and electrons (non-Boltzmann).

The use of truncated ion and electron distributions in a collisionless plasma began with the work of those such as Auer and McIntyre. Auer[12] applies this technique to a plane diode model of a low pressure thermionic convertor but does not provide numerical solutions. In the thermionic convertor, a hot cathode partially ionizes the contained neutral gas and furnishes a plasma which flows to a cold anode. As the applied voltage across the diode and the ratio α of the emitted densities of ions to electrons is varied, a large class of stable and unstable potential profiles is generated. McIntyre[13,14] provides a rigorous charaterization of the profile types possible. Burger[15] utilizes particle simulation to understand the strong oscillations observed experimentally in thermionic convertors operated with ion rich emission. Experimenting with a cesium plasma diode, Ott[16] confirms the collisionless theory for many of the potential configurations. Rynn[17] applies the plane diode model of the thermionic convertor to sheaths in the end columns of a Q-machine. The plasma side of the potential profile away from the emission plate of the Q-machine is assumed by Rynn to have a zero electric field. Kuhn[11] applies the same collisionless model to the single-ended Q-machine to investigate and categorize the strong instabilities observed experimentally.

The above authors apply the kinetic theory to the collisionless plasma region between the source created at the hot emissive surface and the cold collector. We

apply the same theory to a plasma source created in space not at a surface. Hence, the neutralization parameter α (the ratio of emitted ion to electron densities) is not fixed but is dependent on the floating collector potential. (This dependence will be shown later in Sec. II.) With these particular boundary conditions, we extend the kinetic model of Kuhn and those before him to allow unequal ion and electron temperatures.

II. THEORY

A. Model and assumptions

The time-independent behavior of the source and collector sheaths characterizing a bounded, symmetric plasma is modeled as shown in the middle of Fig. 1 over the distance from $x>0$ to the collector at $x=L$. The plasma source at $x=0$ injects temporally constant and equal fluxes of ions and electrons, each with a half-Maxwellian distribution of velocity. The ratio of electron to ion mass, $\mu=m/M$, is a fixed parameter as well as the ratio of ion to electron source temperatures, $\tau=T_{Si}/T_{Se}$. (The parameters μ and τ are consistent with the notations of Kuhn[11] and Emmert *et al.*[2], respectively.)

The plane $x=0$ is at the reference potential of zero. The electric field is zero at $x=0$ because no surface charge is allowed to exist at $x=0$. The collector at $x=L$ electrically floats to potential ϕ_C, absorbs all incident particles which charge the collector, and emits nothing. Net electric current at the collector is zero as the collector is not electrically connected to the external world. Thus the ion and electron fluxes to the collector are equal. The value of potential at the neutral or inflection point, where $\nabla^2\phi=0$, between the source and collector sheaths is designated ϕ_P. The electric field $-\nabla\phi$ at ϕ_P, which by definition is a constant, is chosen to be zero when the source and collector sheaths are many Debye lengths

apart. Thus with the zero source field, the total charge enclosed from $0 \leq \phi \leq \phi_P$ is zero.

In summary, the boundary conditions necessary to solve Poisson's equation for the potential values of ϕ_C and ϕ_P are as follows. The zero reference potential is at $x=0$ where the electric field is zero. The electric field is also zero at ϕ_P. These two conditions of zero field applied to the first integral of Poisson's equation and the neutrality condition at ϕ_P provide two equations with three unknowns: ϕ_C, ϕ_P, and the ratio of emitted densities.

In the plane diode model discussed in Sec. I B, the ratio α of emitted ion to electron densities is specified. For a potential profile that monotonically decreases, assuming that the electric field is zero at $\phi=0$ overspecifies the problem when only ϕ_C and ϕ_P are unknown. In our model, the source density of emitted electrons depends on ϕ_C as caused by the refluxing of repelled electrons at $\phi = 0$. This dependence of α on ϕ_C is found with the third expression which equates the ion and electron currents at $\phi=\phi_C$. Hence, requiring a zero source field with refluxing does not overspecify the problem.

B. Derivation of velocity distributions

The distribution functions $f(x,v)$ for the ions and electrons each satisfy the Vlasov equation. Over the region modeled, the mean free path for collisions is assumed to be much greater than the Debye length of the plasma source. The force applied to each ion or electron is determined with the electric field, $E(x)=-\nabla\phi(x)$, derived with Poisson's equation: $\nabla^2\phi(x)=-4\pi\rho(x)$, where $\rho(x)$ is the net charge density. In time t, the velocity v of each particle of mass m and charge q is governed by the force balance

$$m\frac{dv}{dt} = -q\frac{d\phi}{dx}.$$

Multiplying both sides of this equation by v and rearranging terms provides that

$$\frac{d}{dt}\left(\frac{1}{2}mv^2 + q\phi(x)\right) = 0.$$

Thus expressing each distribution function $f(x,v)$ as a function of this constant of motion, $mv^2/2+q\phi(x)$, satisfies the Vlasov equation. (This proof is found in Nicholson[18].) The velocity distribution functions at any position are then explicitly functions of $\phi(x)$ and the specification of $f(v)$ at a location where ϕ is given.

The electrostatic potential is assumed to be monotonically decreasing with position. Consequently, the velocity distribution of the ions is an accelerated half-Maxwellian governed by conservation of energy; all ions reach the collector. The potential drops near the source and collector repel most of the electrons; only the fastest electrons reach the collector. Hence, the electron velocity distribution is a truncated, decelerated full-Maxwellian following energy conservation. Because all ions injected into the sheath region strike the collector, the slowest ion starting from rest has velocity $V_{Mi}(x)$ given by

$$V_{Mi}(x) = \left(-2e\phi(x)/M\right)^{1/2}$$

where e is unsigned charge of an electron and an ion (singly charged). At any x, the fastest returned electron (which just misses reaching the collector) fixes the minimum velocity $V_{Me}(x)$ given by

$$V_{Me}(x) = -\left[\frac{2}{m}(e\phi(x) - e\phi_C)\right]^{1/2}.$$

Hence, the velocity distribution of the ions, f_i, for a given value of potential is

$$f_i(\psi,v) = N_{Si}\left(\frac{M}{2\pi\tau T_{Se}}\right)^{1/2} \exp\left(-\frac{\psi}{\tau} - \beta_i v^2\right)\Theta(v - V_{Mi}(\psi)). \qquad (1)$$

Similarly the electron velocity distribution function f_e is

$$f_e(\psi, v) = N_{Se}\left(\frac{m}{2\pi T_{Se}}\right)^{1/2} \exp\left(\psi - \beta_e v^2\right)\Theta\left(v - V_{Me}(\psi)\right). \tag{2}$$

For Eqs. (1) and (2) N_{Si} and N_{Se} are the ion and electron densities of the full-Maxwellian source ($x<0$); ψ is the normalized potential $e\phi/T_{Se}$; β_i is $M/(2\tau T_{Se})$ and β_e is $m/(2T_{Se})$; Θ is the Heaviside step function. Hence, for any given value of potential, the shape of the distribution function in the collisionless region is known and its magnitude depends on the source density.

C. Derivation of moments

1. *Definitions*

Determining the first several moments for each species of particles using the distribution functions in Eqs. (1) and (2) provides the potential dependence of each moment. These moments are derived below. The examples shown are for the ions but the same expressions apply for the electrons with obvious changes. Variables for the ions and electrons are named respectively N_i and N_e for particle density, F_i and F_e for particle flux, $\langle V_i \rangle$ and $\langle V_e \rangle$ for drift velocity, T_i and T_e for temperature, Q_i and Q_e for kinetic energy or total energy flux, and H_i and H_e for heat or thermal energy flux. These equations are defined by the following expressions for one dimension.

$$N_i(\psi) = \int_{V_{Mi}(\psi)}^{\infty} f_i(\psi, v)\, dv. \tag{3}$$

$$F_i(\psi) = \int_{V_{Mi}(\psi)}^{\infty} v\, f_i(\psi, v)\, dv. \tag{4}$$

$$\langle V_i(\psi) \rangle = F_i(\psi)/N_i(\psi). \tag{5}$$

$$T_i(\psi) = M\left\langle \left(v - \langle V_i(\psi)\rangle\right)^2 \right\rangle$$

$$= \frac{M}{N_{Si}} \int_{V_{Mi}(\psi)}^{\infty} \left(v^2 - \langle V_i(\psi)\rangle^2\right) f_i(\psi, v)\, dv. \tag{6}$$

$$Q_i(\psi) = \frac{M}{2} \int_{V_{Mi}(\psi)}^{\infty} v^3 f_i(\psi, v)\, dv. \tag{7}$$

$$H_i(\psi) = \frac{MN_{Si}}{2} \left\langle \left(v - \langle V_i(\psi)\rangle\right)^3 \right\rangle$$

$$= \frac{M}{2} \int_{V_{Mi}(\psi)}^{\infty} \left(v^3 - 3\langle V_i(\psi)\rangle v^2 + 2\langle V_i(\psi)\rangle^3\right) f_i\, dv. \tag{8}$$

For electrons, the lower limit of integration is V_{Me}, a negative value. Additional energy fluxes are defined in detail by Shkarofsky *et al.*[19]

2. *Densities and particle fluxes*

An evaluation of the first velocity moments with Eq. (4) for ions and electrons shows that F_i and F_e are spatially constant. With no creation or annihilation of particles along $0 < x < L$ then conservation of particles requires that

$$\frac{\partial N}{\partial t} + \nabla \cdot \mathbf{F} = 0.$$

In our one-dimensional system, when the loss rate at the collector equals the injection rate at the source then $\partial N/\partial t = 0$ so that $\mathbf{F}$ is spatially constant for each species.

The fluxes injected from the source are assumed temporally constant and equal for both species; hence we may equate the net fluxes to the injected flux with $F_i(\psi) = F_e(\psi) = F$. Evaluating Eq. (4) from $V_M(x)$ to ∞ for the ions and electrons gives the net fluxes as

$$F_i = N_{Si}\left(\frac{\tau T_{Se}}{2\pi M}\right)^{1/2} \tag{9}$$

and

$$F_e = N_{Se}\left(\frac{T_{Se}}{2\pi m}\right)^{1/2} \exp\psi_C. \tag{10}$$

Hence, the presence of refluxed electrons increases the source density N_{Se} (and the magnitude of $f_e(x,v)$) by a factor of $\exp(-\psi_C)$. Equivalently, the flux of electrons emitted from the source (only $v>0$) equals $F_e \exp(-\psi_C)$. The ion source density (and magnitude of $f_i(x,v)$) is unaffected by ψ_C because all ions reach the collector and so do not return with information about the downstream potential.

Equating Eq. (9) with Eq. (10) satisfies the zero current condition at the collector for the open-circuited system and fixes the ion to electron density ratio of the source (not at $\psi=0$) so that

$$N_{Si}/N_{Se} = (\mu\tau)^{-1/2} \exp\psi_C.$$

The ratio of N_{Si}/N_{Se} also equals the ratio of outgoing densities (with $v>0$) emitted from the source which includes the refluxed contribution. This ratio equals the neutralization parameter α for our particular boundary conditions. As discussed in Sec. I B, the neutralization parameter is used by previous authors[11-17] in characterizing the emission from the hot cathode of a thermionic emitter or Q-machine. Our value of α is usually greater than one, which suggests an "ion rich" source of emission. This terms implies that the potential curvature, $\nabla^2\phi$, at $x=0$ is negative even though the electric field, $-\nabla\phi$, at $x=0$ is zero.

The integrals of Eq. (3) are evaluated next to obtain ion and electron densities with the dependence on injected flux F from Eqs. (9) and (10). The resulting densities, which depend on the potential profile, can be now expressed as

$$N_i(\psi) = F\left(\frac{\pi M}{2\tau T_{Se}}\right)^{1/2} \exp(-\psi/\tau)\mathrm{erfc}(-\psi/\tau)^{1/2} \tag{11}$$

and

$$N_e(\psi) = F\left(\frac{\pi m}{2T_{Se}}\right)^{1/2} \exp(\psi - \psi_C)\left[1 + \mathrm{erf}(\psi - \psi_C)^{1/2}\right]. \tag{12}$$

At first reading, this form for $N_e(\psi)$ appears different from the simple Boltzmann factor for electron density. This difference occurs because our model uses a constant injected particle flux; other models use a constant background density. If the electrons are assumed to have a full-Maxwellian distribution, then $-V_{Me} \to \infty$, which occurs as $M/m \to \infty$. Applying Eq. (3) to these electrons expresses the Boltzmann electron density $N_B(\psi)$ as

$$N_B(\psi) = F\left(\frac{2\pi m}{T_{Se}}\right)^{1/2} \exp(\psi - \psi_C) \tag{13}$$

or with Eq. (10),

$$N_B(\psi) = N_{Se} \exp(\psi).$$

For our model, as ψ_C changes with the mass and temperature ratios of the plasma source and for the same injected particle flux, the value of $N_B(0)$ will change according to Eq. (13). Previous analyses[4,7–9] assume that ion and electron source densities are equal and fixed which causes F to be the variable parameter. However, an investigation of the temporal evolution of the system to some equilibrium state suggests that the injection flux be fixed and the source density be determined self-consistently.

3. *Temperature*

Using the definition of drift velocity in Eq. (5) and the above derivations in Eqs. (11) and (12) for density, one observes that the drift velocity is dependent on source temperature but independent of injected flux. With this drift velocity and the second velocity moment, the "effective" temperature is derived. The concept

of temperature is usually applied to collisional plasmas with full Gaussian distributions. For our model of the collisionless sheath, we use temperature as the mean square deviation given in Eq. (6). Evaluating Eq. (6) gives the ion and electron temperature dependence on potential as

$$\frac{T_i(\psi)}{\tau T_{Se}} = \frac{1-(2/\pi)^{1/2}M^{3/2}(\tau T_{Se})^{-3/2}G(\beta_i, V_{Mi}(\psi))}{\mathrm{erfc}(-\psi/\tau)^{1/2}} - \frac{2\exp(2\psi/\tau)}{\pi\left[\mathrm{erfc}(-\psi/\tau)^{1/2}\right]^2} \tag{14}$$

and

$$\frac{T_e(\psi)}{T_{Se}} = \frac{1+(2/\pi)^{1/2}m^{3/2}T_{Se}^{-3/2}G(\beta_e, V_{Me}(\psi))}{1+\mathrm{erf}(\psi-\psi_C)^{1/2}} - \frac{2\exp(2\psi_C-2\psi)}{\pi\left[1+\mathrm{erf}(\psi-\psi_C)^{1/2}\right]^2} \tag{15}$$

where

$$G(\beta, y) = \int_0^y v^2 \exp\left(-\beta v^2\right) dv.$$

The above normalized temperatures, independent of source temperatures T_{Se} and τT_{Se}, depend only on ψ, ψ_C, μ, and τ. Note that at the collector $T_e(\psi_C) = T_{Se}(1-2/\pi)$ and at $\psi=0$ (just within the collisionless source sheath region) $T_i(0) = \tau T_{Se}(1-2/\pi)$. This sharp jump down in $T_i(0)$ occurs because at $x=0$, temperature indicates the mean square deviation in the half-Maxwellian velocity distribution; whereas, the ion source temperature τT_{Se} indicates that of the full-Maxwellian velocity distribution.

The temperature expressions in Eqs. (14) and (15) are written so that the first terms are equal to $M\langle V_i^2\rangle/\tau T_{Se}$ and $m\langle V_e^2\rangle/T_{Se}$ and the second terms are equal to $M\langle V_i\rangle^2/\tau T_{Se}$ and $m\langle V_e\rangle^2/T_{Se}$. The values obtained for $\langle V_i^2\rangle$ and $\langle V_i\rangle^2$ (normalized

to V_{ti}^2) at the locations of ψ_C and ψ_P for $\mu = 1/1836$ are listed in Table I. (These expressions for ψ_C and ψ_P will be discussed in Sec. II D.) Using 16 significant digits of accuracy for the terms in Eq. (14), we find that these expressions can be evaluated for $|\psi_C/\tau| \leq 30$ which corresponds to $1/9400 \leq \mu\tau \leq 1$. Smaller values of $\mu\tau$, such as $\mu = 1/1836$ and $\tau = 0.1$, require 32 significant digits to evaluate $\langle V_i^2 \rangle$ and $\langle V_i \rangle^2$ accurately. Table I is presented primarily to compare our results on the ion drift velocity entering the collector sheath with the conclusions from other authors. This comparison will be discussed in detail in Sec. V.

4. *Energy flux*

Evaluating Eq. (7) to obtain the third moment of the velocity distributions produces the kinetic energy fluxes as

$$Q_i(\psi) = \tau F T_{Se}(1 - \psi/\tau) \tag{16}$$

and

$$Q_e(\psi) = F T_{Se}(1 + \psi - \psi_C). \tag{17}$$

Note that while each energy flux varies with distance, the sum of $Q_i(\psi)$ and $Q_e(\psi)$ is independent of position. Even when particles have a full-Maxwellian velocity distribution in the other two dimensions, this spatial dependence holds true for the total kinetic flux along x.

The kinetic energy flux divided by the particle flux is defined as the mean kinetic energy.[9] Thus the ions arrive at the collector with a mean kinetic energy of $\tau T_{Se}(1 - \psi_C/\tau)$ and the electrons arrive with a mean kinetic energy of T_{Se}. Note that the mean kinetic energy of the incident stream is not the same as the stream temperature which indicates the spread about the drift velocity.

Lastly the heat flux of each species is evaluated. As expressed in Eq. (8), heat flux indicates the thermal flow of thermal energy which contributes in part to the

TABLE I. Ion kinetic energy and drift energy from our theory and previous analyses at various locations with $M/m = 1836$. Energies are normalized to the square of the ion thermal velocity V_{ti}^2 at the source. The following are the expressions used in the previous analyses to derive the limits shown below. Bohm[4]: $\langle V_i^2 \rangle V_{ti}^{-2} \geq \tau^{-1}$. Stangeby[7]: $\langle V_i \rangle^2 V_{ti}^{-2} \geq \tau^{-1} + 1$. Chodura[9]: $\langle V_i \rangle^2 V_{ti}^{-2} \geq \tau^{-1} + 5/3$.

		Temperature Ratio, $\tau = T_{Si}/T_{Se}$				
Theory	$\tau = 0.1$		$\tau = 1$		$\tau = 10$	
Our Analysis						
Location:	x_P[a]	x_C[b]	x_P	x_C	x_P	x_C
Potential: $-\psi(x,\tau)$	0.85	3.38	0.34	2.86	0.05	1.91
$\langle V_i^2(\psi) \rangle V_{ti}^{-2}$	18.9	69.6	2.14	7.52	1.09	1.76
$\langle V_i(\psi) \rangle^2 V_{ti}^{-2}$	18.9	69.6	1.92	7.43	0.74	1.51
Previous Analyses						
Location:	Entering the collector sheath edge (presumably between x_P and x_C).					
Bohm:	$\langle V_i^2 \rangle V_{ti}^{-2}$	≥ 10.0		≥ 1.0		≥ 0.1
Stangeby:	$\langle V_i \rangle^2 V_{ti}^{-2}$	≥ 11.0		≥ 2.0		≥ 1.1
Chodura:	$\langle V_i \rangle^2 V_{ti}^{-2}$	≥ 11.7		≥ 2.7		≥ 1.8

[a] Position x_P is where $\nabla^2 \psi_P = 0$ and $-\nabla \psi_P = 0$.

[b] Position x_C is where $\psi = \psi_C$ at the electrically floating collector.

kinetic energy flux. The heat flux H is evaluated exactly in terms of the previously derived profiles for the ions as

$$H_i(\psi) = Q_i(\psi) - 3FT_i(\psi)/2 - FM\langle V_i(\psi)\rangle^2/2 \tag{18}$$

and for the electrons as

$$H_e(\psi) = Q_e(\psi) - 3FT_e(\psi)/2 - Fm\langle V_e(\psi)\rangle^2/2. \tag{19}$$

D. Derivation of collector potential and source sheath potential drop

In a fully kinetic model of the axially symmetric Q-machine, Kuhn[11] evaluates values of potential at extrema and inflection points along the region modeled for equal source fluxes and temperatures. When N_{Si}/N_{Se}, our neutralization parameter, is plotted against ψ_C with $\tau = 1$ for various μ in Fig. 4 of Kuhn's paper, the results lie on the boundary (curve C′) which separates the "one-maximum" and "monotonically decreasing" types of potential profiles. The zero field condition at the source places the one-maximum point in the potential at $x = 0$. This gives our model with $\tau = 1$ the attributes of both profile types. We next extend the model of Kuhn for our boundary conditions to allow for source temperature ratios other than unity.

With reference to the middle sketch of Fig. 1, the potential is characterized by $\nabla^2\psi_P = 0$ somewhere between the source and collector sheaths. Hence setting the net charge density to zero finds this inflection point. Equating $N_i(\psi_P)$ and $N_e(\psi_P)$ from Eqs. (11) and (12), derives the neutrality expression which relates ψ_C and ψ_P:

$$\frac{1}{\sqrt{\mu\tau}}\exp\left(\frac{-\psi_P}{\tau}\right)\operatorname{erfc}\left(\frac{-\psi_P}{\tau}\right)^{1/2} = \exp(\psi_P - \psi_C)\left[1 + \operatorname{erf}(\psi_P - \psi_C)^{1/2}\right]. \tag{20}$$

Recall that the assumption of zero net electric current (floating collector) has been included in the solution for these densities.

A second equation relating ψ_C and ψ_P results from imposing the zero electric field condition at the inflection point ψ_P. Integrating Poisson's equation, $\nabla^2\psi = 4\pi e^2 T_{Se}^{-1}(N_e - N_i)$, once from $\psi = 0$ to $\psi = \psi_P$ and applying the two field boundary conditions is equivalent to integrating Eq. (20). The resulting expression can be written in separate terms of the normalized integral densities $\mathcal{I}$ for ions and electrons which are respectively,

$$\mathcal{I}_i = \sqrt{\frac{\tau}{\mu}}\left[\exp\left(\frac{-\psi_P}{\tau}\right)\mathrm{erfc}\left(\frac{-\psi_P}{\tau}\right)^{1/2} - 1 + \left(\frac{-4\psi_P}{\pi\tau}\right)^{1/2}\right],$$

and

$$\mathcal{I}_e = \exp(\psi_P - \psi_C)\left[1 + \mathrm{erf}(\psi_P - \psi_C)^{1/2}\right] + \frac{2}{\sqrt{\pi}}(-\psi_C)^{1/2} - \frac{2}{\sqrt{\pi}}(\psi_P - \psi_C)^{1/2} - \exp(-\psi_C)\left[1 + \mathrm{erf}(-\psi_C)^{1/2}\right].$$

Thus the zero electric field condition at ψ_P is that the normalized integral densities sum to zero,

$$\mathcal{I}_i + \mathcal{I}_e = 0. \tag{21}$$

Together, Eqs. (20) and (21) define the source sheath drop ψ_P and collector potential ψ_C in terms of the mass and temperature ratios.

For the special case of cold ions, i.e., $\tau = 0$, (with no initial drift velocity) these two equations are satisfied as both ψ_C and ψ_P go to $-\infty$. To satisfy the zero total current condition when $\tau = 0$, the ion density at the source must be infinite which generates an infinitely large potential drop across the source sheath.

The form of the dependence of ψ_C on ψ_P from Eqs. (20) and (21) is the same for most values of μ and τ. In Fig. 2 we plot a typical curve from each equation for $\mu = 1/1836$ and $\tau = 1$, which Kuhn's results also yield. The simultaneous solution

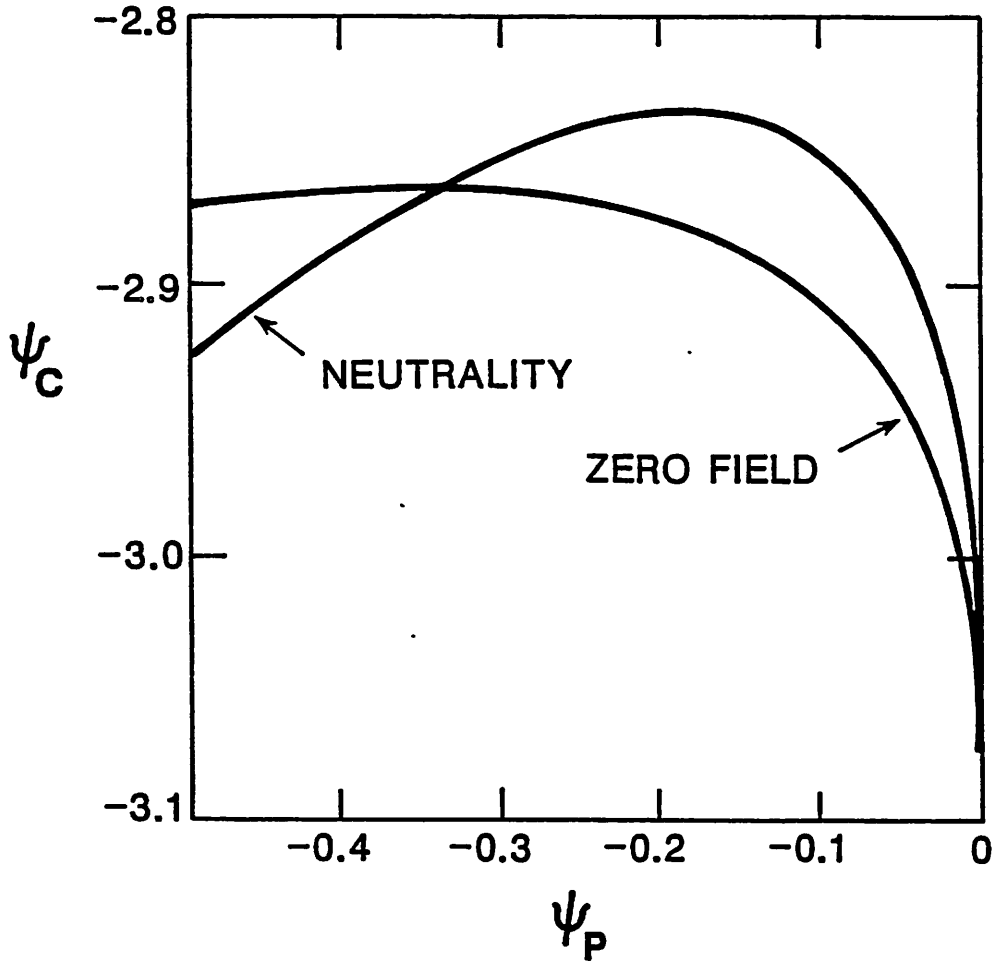

FIG. 2. Solutions of ψ_C *vs.* ψ_P for the neutral charge density ρ expression in Eq. (20) and the zero field condition in Eq. (21) using $M/m = 1836$ and $T_{Si}/T_{Se} = 1$ at the source. The potentials are normalized as $\psi = e\phi/T_{Se}$.

for these equations exists at two points. The first occurs where $d\psi_C/d\psi_P = 0$ for Eq. (21). Differentiating Eq. (21) expresses $d\psi_C/d\psi_P$ in the form of

$$A(\psi_C, \psi_P)\frac{d\psi_C}{d\psi_P} + N_e(\psi_C, \psi_P) - N_i(\psi_P) = 0.$$

This equation is satisfied when $N_i = N_e$ and $d\psi_C/d\psi_P = 0$. We find that our particle simulations always evolve to solutions matching the first type of intersection point. Kuhn[20] also solves for ψ_C from this first intersection point in characterizing the boundary between the monotonically decreasing and the one-maximum profiles.

The second point of solution occurs where $\psi_P = 0$ for both equations. Although ψ_C is fixed by Eq. (20) when $\psi_P = 0$, any value of ψ_C satifies Eq. (21) when $\psi_P = 0$. It would seem that sheath analyses which neglect the "presheath" potential drop would encompass this type of solution. However, values for ψ_C from these analyses are actually much less in magnitude than ψ_C from our solution with $\psi_P = 0$. Although this second intersection point is a solution to both equations, it may not provide a temporally stable profile when the plasma is perturbed.[20]

The simultaneous solutions of Eqs. (20) and (21) are represented by plots of ψ_C and ψ_P as a function of mass ratio for three temperature ratios, $\tau = 0.1$, 1, and 10 in Fig. 3(a). With the same technique for the particular mass ratio of a hydrogen plasma, the dependence of ψ_C and ψ_P on temperature ratio is shown in Fig. 3(b). Both plots are obtained from solutions of the first type of intersection point mentioned above. Observe that the potential drop through the source sheath varies primarily with τ (seen in Fig. 3(b)) but very little with mass ratio (seen in Fig. 3(a)). This method of solution realistically models a wide range of mass and temperature ratios. For $\mu = 0.1$ and $\tau = 10$, i.e., equal ion and electron thermal velocities, the potential profile is flat, occuring whenever $\mu\tau = 1$. Analyses which assume a Boltzmann electron density show erroneously that $\psi_C > 0$ for $\mu\tau = 1$, as will be discussed in Sec. IV B.

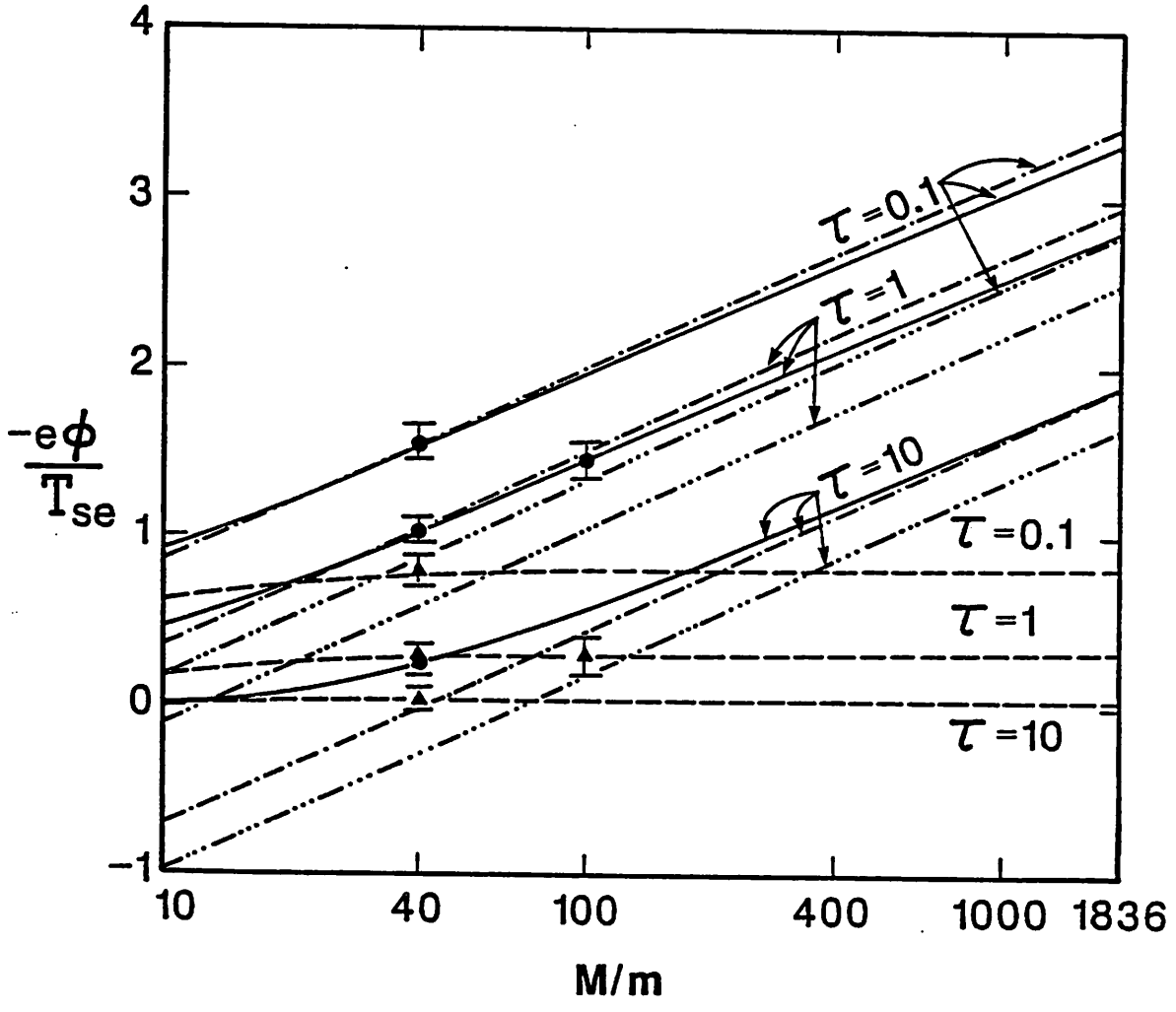

FIG. 3(a). Potential at various locations as a function of mass ratio, $1/\mu$, for three source temperature ratios $\tau = T_{Si}/T_{Se}$. Collector potential $\psi_C(\tau)$ (solid curves) and source sheath potential drop $\psi_P(\tau)$ (dashed curves) are from our kinetic theory. Results of Emmert *et al.*[2] for $\psi_C(\tau)$ (dot-dashed lines) are derived with the values of $\psi_1(\tau)$ at the collector sheath edge shown in Fig. 3(b). Also plotted is the solution by Stangeby[7] (triple-dot dashed lines) for the collector sheath drop, $\psi_f = 0.5 \ln(2\pi\mu(1+\tau))$. Simulation data points of $\psi_C(\tau)$ (circles) and $\psi_P(\tau)$ (triangles) are measured at $x = 0.5L$ and L, respectively. Bars indicate oscillation amplitudes of ψ.

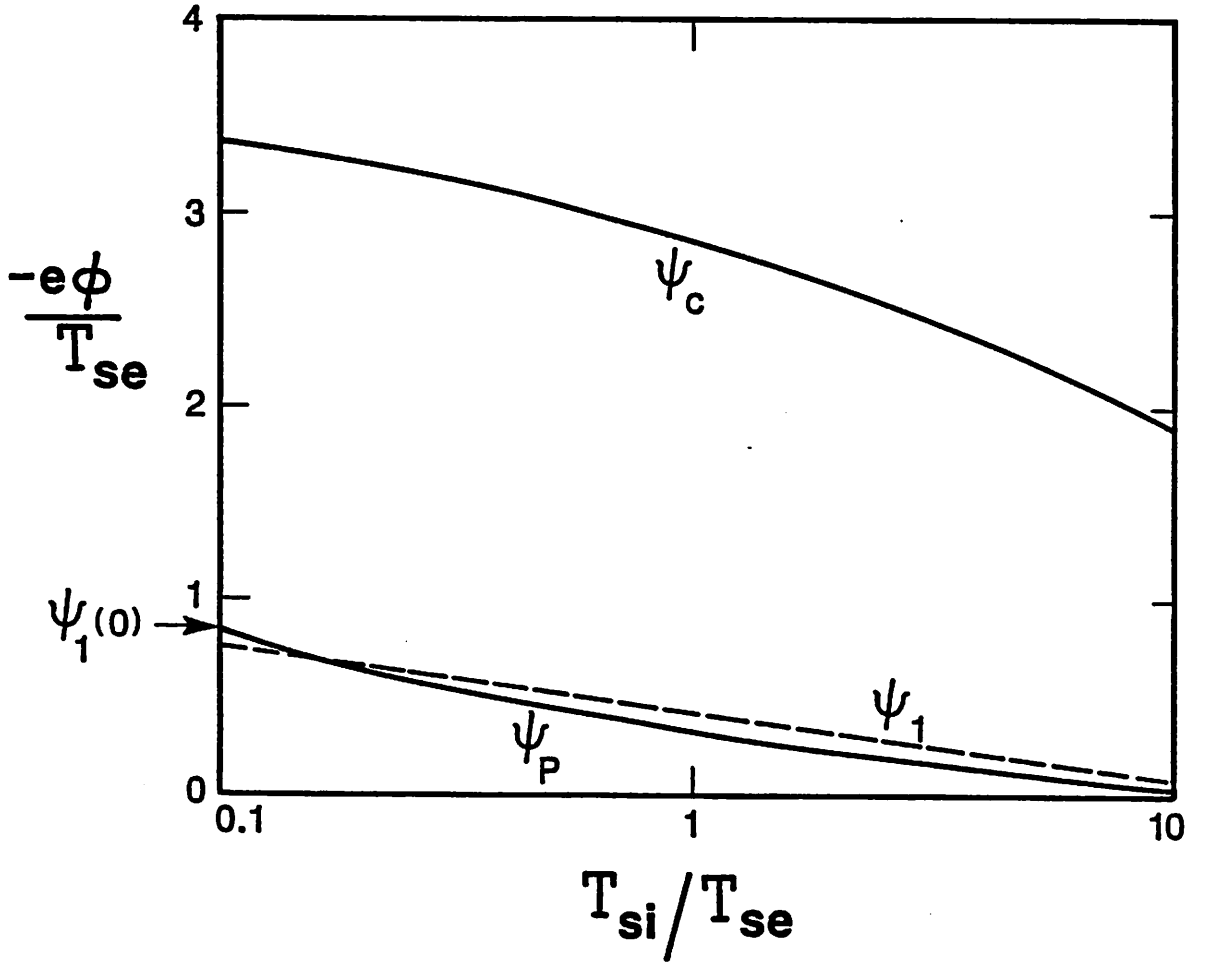

FIG. 3(b). Potentials at various locations as a function of temperature ratio, T_{Si}/T_{Se}, at $M/m = 1836$. Collector potential $\psi_C(\tau)$ and source sheath potential drop $\psi_P(\tau)$ (solid curves) are from our kinetic theory. Potential at the collector sheath edge, $\psi_1(\tau)$, (dashed line) is that from Emmert *et al.*[2]

III. PARTICLE SIMULATIONS

A. Simulation description and fixed parameters

A particle-in-cell computer simulation for ions and electrons is used to study the region between a Maxwellian plasma source and a purely absorbing collector. The Lorentz equation of motion is integrated twice to move the particles. The electric fields are obtained self-consistently on a fixed mesh by solving Poisson's equation for potential in each time step. The simulation region of $0 \leq x \leq L$, shown at the bottom of Fig. 1, is initially empty. Particle electrons and ions with an inverse mass ratio μ of 1/40 or 1/100 are injected with equal and temporally constant fluxes. (Because computation time increases with mass ratio and our allocation of Cray computation time is limited, mass ratios for a hydrogen plasma are not utilized in these simulations.)

Both ions and electrons enter the region with a half-Maxwellian velocity distribution with temperature ratios τ of 0.1, 1, or 10. Electrons which return to the source at $x = 0$ are "refluxed", i.e. re-inserted as injected particles with a velocity characteristic of the electron source temperature. Consequently the net electron emission rate (those with $v > 0$ at $x = 0$) exceeds that of the ions. Because of this refluxing, no charge accumulation is allowed at the source plane; hence, the electric field at $x = 0$ is zero. At $x = L$, incident particles are absorbed and charge the collector which is electrically floating.

B. Variable parameters

Spatial profiles are presented for the velocity scatter, electrostatic potential, and various moments of the velocity distribution. The profiles are evaluated after the average number of particles in the system becomes approximately constant with time. These moments are discussed earlier in Sec. II C 1 and defined in Eqs. (3)–(8).

Particles are linearly weighted to each grid where the velocity distributions and moments are evaluated. Maximum velocity values injected at the source are six times the thermal velocity. Methods used are described in Birdsall and Langdon's book[21]. The code used here is fundamentally PDW1 composed by Lawson,[22] with transport evaluation added.

Relevant simulation parameters are described below. Systems studied are from 20 to 50 Debye lengths (λ_D) long and are resolved with about 6 grid points per λ_D. A density of at least 400 particle electrons in $1\lambda_D$ is required for reduction of potential fluctuations to within $\pm 10\%$. Time steps are typically $0.05/\omega_P$, where ω_P is the spatially averaged plasma frequency.

C. Transient behavior of the collector potential with various temperature ratios

The temporal behavior of the collector potential with $\tau = 0.1$, 1, and 10 is displayed with the time history plots shown in Fig. 4. Typically ψ_C fluctuates with frequency ω_P which depends on the time-dependent N_e in the system. For each case, the calculated value of ten plasma periods T_{pe} is indicated by double arrows. In this figure, the collector potential begins at zero and then dips to 4–8 times the final, averaged value of ψ_C. The most negative value of ψ_C occurs when the electrons, with a velocity of 1.5–2.0 V_{te} where $V_{te}=(T_{Se}/m)^{1/2}$, reach the collector. As incoming ions begin to neutralize the large initial negative charge at the collector, then ψ_C increases to the equilibrium value in 3–4 transit times of an ion traveling with velocity $V_{ti}((2/\pi) + (-2\psi_C/\tau))^{1/2}$ where $V_{ti} = (\tau T_{Se}/M)^{1/2}$. By this time of potential equilibration, the ion and electron fluxes are spatially equal; however, the fluxes themselves are not yet constant in space. The fluxes become spatially constant in 15–20 times $L(-\psi_C)^{-1/2}V_{te}^{-1}$. At this same time, by conservation of particles (discussed in Sec. II C 2), the total number of system particles becomes

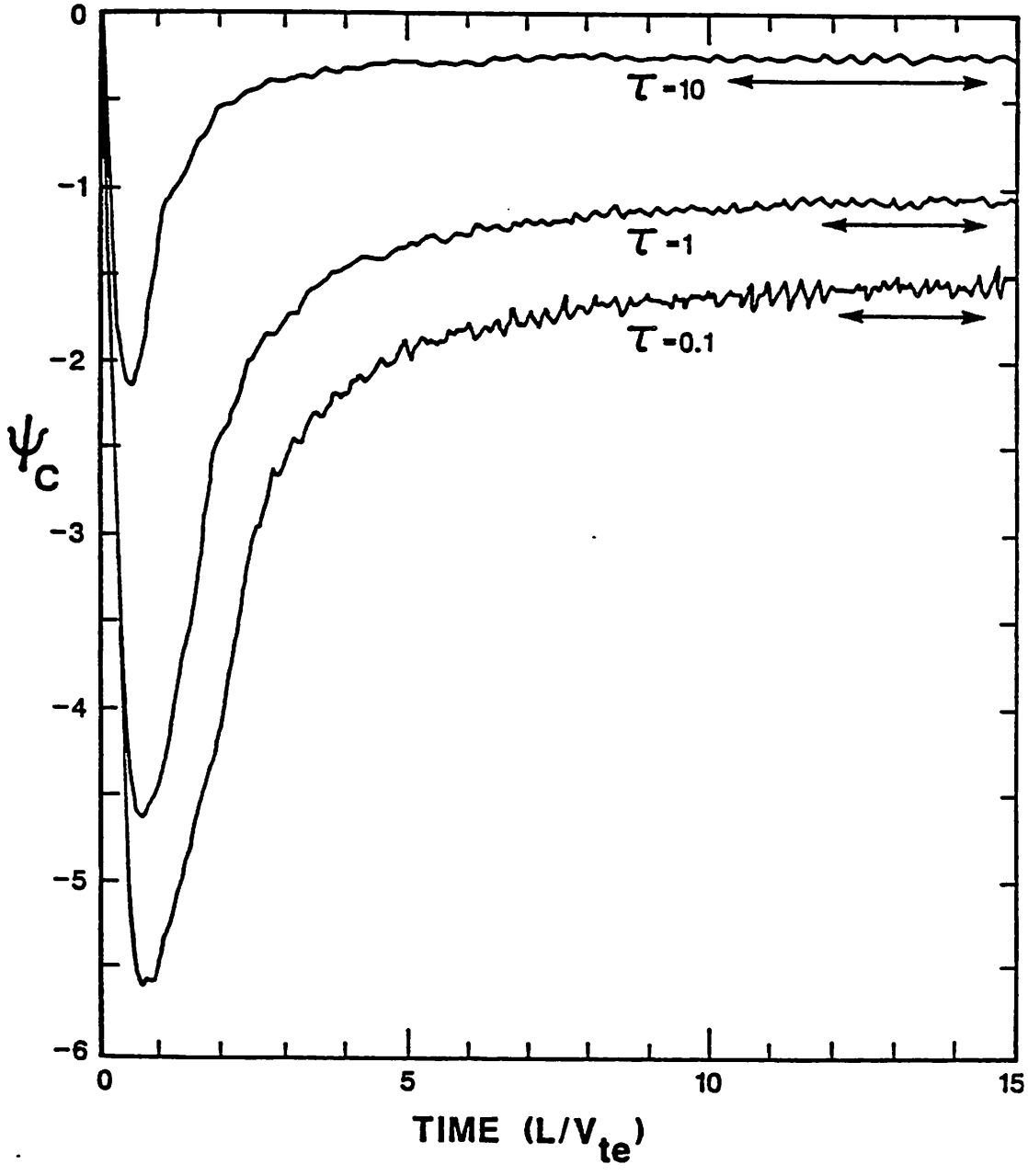

FIG. 4. History of collector potential from simulation for $M/m = 40$ and three source temperature ratios $\tau = T_{Si}/T_{Se}$. For $\tau = 0.1$ and 1, the system length $L = 22\lambda_D$ and for $\tau = 10$, $L = 15\lambda_D$. Double arrows indicate the calculated value of ten plasma periods T_{Pe}, determined from the length-averaged electron density. Normalized potential, $\psi_C = e\phi_C/T_{Se}$, is measured at $x = L$.

temporally constant. All plots shown hereafter are obtained at a time after particle equilibration.

D. Simulation results with a temperature ratio of unity at steady state

1. *Potential profiles and velocity distributions*

The family of spatial profiles shown in Figs. 5(a)–5(h) are generated via particle simulation using $\mu = 1/40$, $\tau = 1$, and a length of $44\lambda_D$. The phase spaces (scatter plots) of ions and electrons along x are shown in Figs. 5(a) and 5(b); also included are the velocity distribution functions $f(v)$ for both species at four values of x as obtained and smoothed from the scatter plots. The ions are accelerated throughout the region and all reach the collector. Only the fastest electrons reach the collector; the remaining slower electrons are repelled by the source and collector potential drops. A distinct cut-off electron velocity $V_{Me}(x)$ is observed. We observe no collisional or collective processes which scatter particle electrons beyond $V_{Me}(x)$ to fill in the "missing tail" during the time of our simulations. These processes are hypothesized to explain the Langmuir paradox.[23]

The potential profile which evolved with these velocity distributions is presented in Fig. 5(c). Both the potential profile and scatter plots are snapshots at the last time step of the simulation. The spatial lengths of the source and collector sheaths are approximately $4\lambda_D$. The potential profile is quite flat (i.e., $-\nabla\psi \approx 0$) between the sheaths when we use at least $N_D = 400$ particle electrons in one λ_D where $N_D = N_e\lambda_D$ averaged along x in one dimension. Smaller values of N_D produce a small positive electric field between both sheaths. With a positive curvature in potential at the plasma edge of the source sheath and a negative curvature entering the collector sheath, an inflection point in potential occurs between the two sheaths. (With the zero field condition imposed at the source, potential curvature there is negative. Thus another inflection points occurs midway in the source

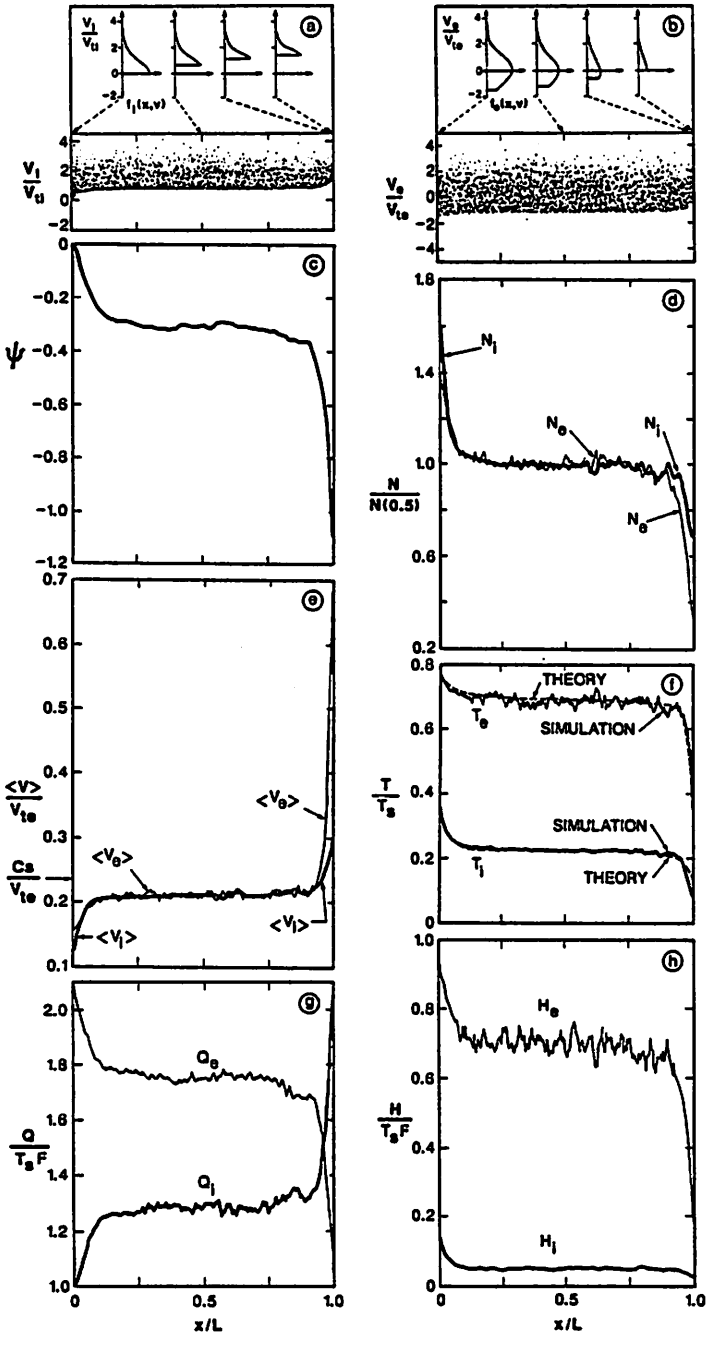

FIG. 5. Spatial profiles from simulation with $M/m=40$, $T_{Si}/T_{Se}=1$, and $L=44\lambda_D$ of (a) ion and (b) electron velocity scatter plots with f(v) from four locations, (c) normalized potential, and, for both species, normalized profiles of (d) density, (e) drift velocity, (f) temperature, (g) kinetic energy flux, and (h) heat flux. (T_S is equivalent to T_{Se}.)

sheath.) Hence our earlier descriptions of $\nabla^2\psi_P = 0$ and $-\nabla\psi_P = 0$ are valid. The spatial ripples in potential are roughly $1\,\lambda_D$ in length and are associated with small oscillations and waves with the plasma frequency ω_P.

To understand the effect of refluxing in our simulations, we model the following test case. No refluxing is allowed so that the surface at $x = 0$ is charged or discharged by incident or emitted particles. As derived in Sec. II C 2, the electron flux emitted from the source is $F\exp(-\psi_C)$ for our original boundary conditions. Consequently, the ratio of the flux of emitted ions to electrons is set to a temporally constant value of $\exp(\psi_C)$. This value of ψ_C is found from Fig. 3(a) for the mass and temperature ratios of the simulation. All other conditions in the test case are identical to those of the original. This test case is observed to produce the same potential profile and level of fluctuations as generated with the original conditions with refluxing. Hence our refluxing mechanism allows this excessive electron emission to occur self-consistently without causing additional, artificial fluctuations.

2. *Profiles of velocity moments*

The spatial profiles of each species for density, drift velocity, temperature, kinetic energy flux, and heat flux are discussed next. Shown in Figs. 5(d)–5(h), all of these profiles are time-averaged over a plasma period prior to the last time step. The ion and electron density profiles in Fig. 5(d) are each normalized to their central density at $x/L = 0.5$. The collector sheath and region of the source sheath adjacent to the source are characterized by $N_i > N_e$. Over the central region between the sheaths, $N_i \approx N_e$.

The ion and electron profiles of drift velocity, each normalized to the electron thermal velocity V_{te}, are shown in Fig. 5(e). In these profiles, $\langle V_e\rangle > \langle V_i\rangle$ in the ion rich region of both sheaths, as described above. Multiplying densities from Fig. 5(d)

with velocities from Fig. 5(e), it appears that particle flux, $F=N\langle V\rangle$, is conserved and equal for both species.

Effective ion and electron temperature profiles normalized to the electron source temperature T_{Se} are shown in Fig. 5(f). The ion temperature T_i decreases along x because the decreasing potential accelerates and thus cools (reduces the velocity spread about the mean) the velocity distribution as seen in Fig. 5(a). At $x=0$, T_i drops abruptly from τT_{Se} due to the discontinuity between the assumed full-Maxwellian at $x<0$ and the injected half-Maxwellian at $x=0$, both with the same $\exp(-v^2/(2V_{te}^2))$ distribution. The electron temperature $T_e(x)$ decreases from T_{Se} because the magnitude of the cut-off velocity decreases with x as seen in Fig. 5(b). At $x=0$, T_e drops abruptly from T_{Se} because $f_e(0,v)$ is not quite a full Maxwellian distribution. As shown in Sec. II C 3, for $\tau=1$, $T_e(\psi_C)=T_i(0)=0.36$ which is verified with Fig. 5(f).

The ion and electron profiles of kinetic energy flux are plotted in Fig. 5(g). The value of total kinetic energy flux at the collector, normalized by $T_{Se}F$, is sometimes referred to as δ_t, the energy or power transmission factor[7] where

$$\delta_t = \big(Q_i(\psi_C)+Q_e(\psi_C)\big)/(T_{Se}F).$$

Using Q/F as mean kinetic energy[9], the curves in Fig. 5(g), multiplied by T_{Se}, yield profiles of mean kinetic energy. This figure shows that ions deposit twice as much total energy at the collector as do electrons. More generally from Eqs. (16) and (17) at the collector, $Q_i/Q_e=\tau-\psi_C$. This ratio is 2.04 for $\mu=1/40$ and $\tau=1$; for a Maxwellian distribution, this ratio is 2.

The last velocity moment is heat flux, i.e., the thermal flow of thermal energy. These profiles, also normalized by $T_{Se}F$, are shown for each species in Fig. 5(h). The heat flux at the collector due to ions is less than that due to electrons because

the ions have less thermal spread and so less thermal energy to transfer. The heat flux profiles can be determined from the profiles in Figs. 5(e)–5(g) using Eqs. (18) and (19). Both kinetic energy flux and heat flux are plotted in Figs. 5(g) and 5(h) to point out their difference; occasionally authors define the third velocity moment and then inappropriately refer to it as heat flux.

E. Simulation results with various temperature ratios at steady state

The effect of temperature ratio τ on potential and on ion drift velocity profiles are evaluated briefly. With the electron source temperature fixed, increasing the ion source temperature decreases the magnitude of potential drop across the region. This trend is illustrated with three simulations using $\tau = 0.1$, 1, and 10 with lengths of $22\,\lambda_D$, $22\,\lambda_D$, and $15\,\lambda_D$, respectively. Snapshots of the potential profiles from the last time step are shown in Fig. 6. The potential drops through both the source sheath and the collector sheath increase as τ is reduced (ions cooled). With smaller τ (and equal injected fluxes), $N_i(0)/N_e(0)$ is greater. This increasing density ratio generates a steeper potential profile (greater negative curvature in $\psi(x)$) leaving the source. In the extreme case, as $\tau \rightarrow 0$, the model with no ion drift velocity away from the source region (where $-\nabla\psi(0) = 0$) would be difficult to simulate because $\psi_P \rightarrow -\infty$.

The ion drift velocity increases with distance from the source. When τ is reduced, the entire profile of ion drift velocity also increases. Both trends are illustrated in Fig. 7 which contains profiles of ion drift velocity normalized by the ion thermal velocity V_{ti}, using results from the same three simulations used in Fig. 6. These plots of ion drift velocity are time-averaged over a plasma period prior to the last time step. Note also in Fig. 7, that the value of $\langle V_i(0) \rangle$ for each τ equals $V_{ti}(2/\pi)^{1/2}$ as predicted in the solution obtained by substituting Eq. (13) with $\psi = 0$ into Eq. (5).

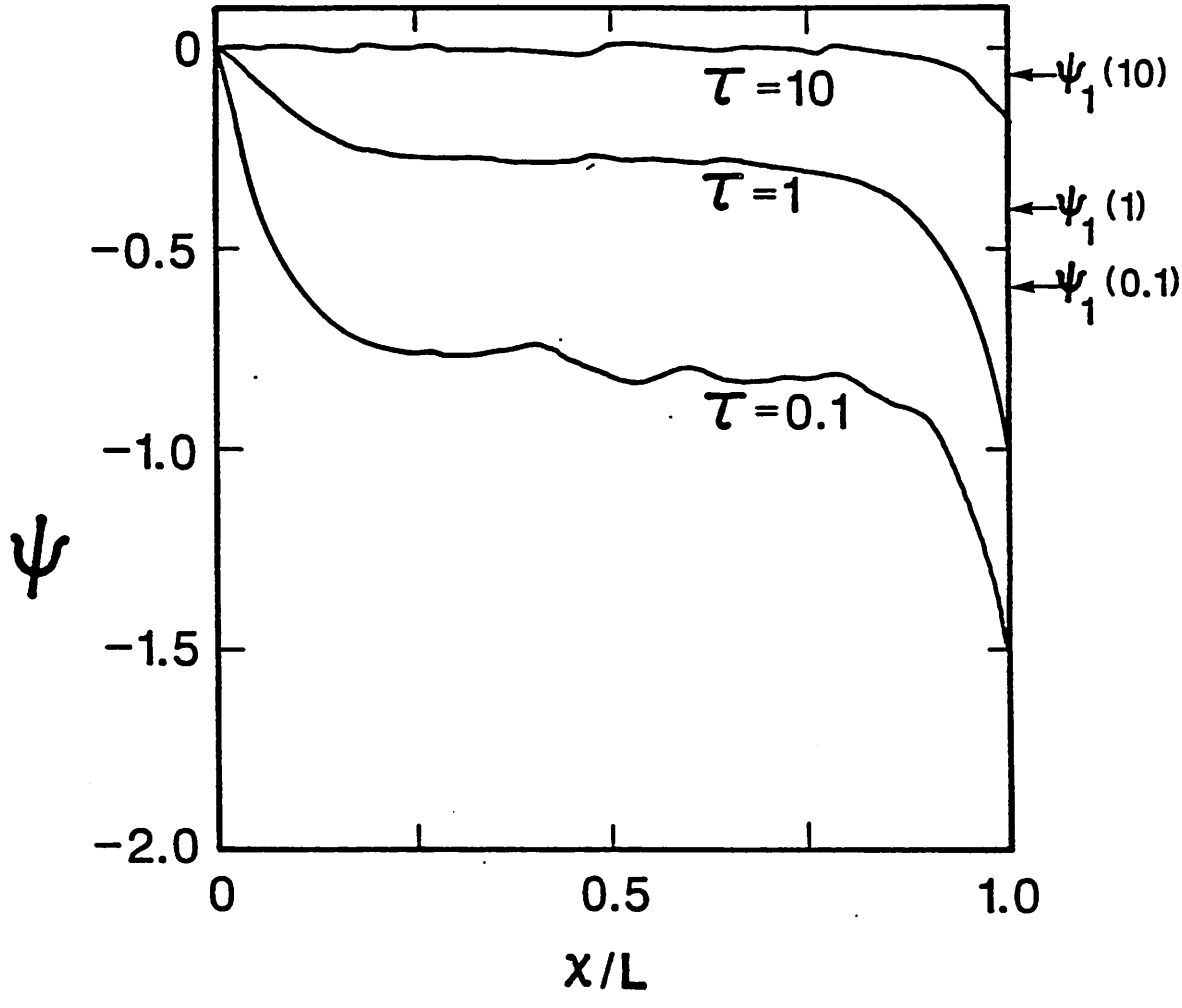

FIG. 6. Potential profiles from simulation with $M/m = 40$ for three temperature ratios $\tau = T_{Si}/T_{Se}$ at the source. For $\tau = 0.1$ and 1, $L = 22\lambda_D$ and for $\tau = 10$, $L = 15\lambda_D$. Also indicated are $\psi_1(\tau)$ at the plasma-sheath boundary from Emmert *et al.*[2] The potentials are normalized as $\psi = e\phi/T_{Se}$.

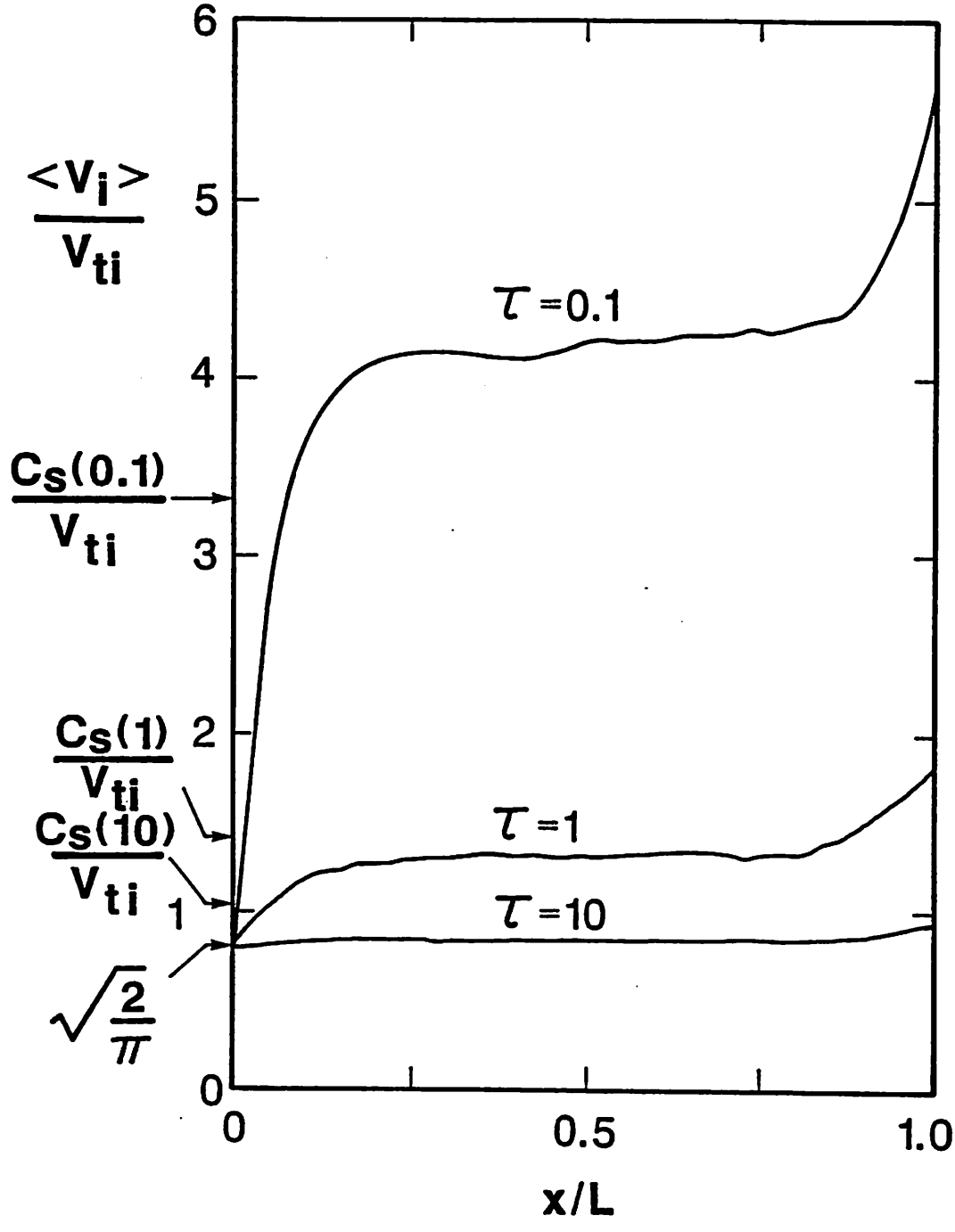

FIG. 7. Profiles of ion drift velocity from simulation with $M/m = 40$ for three temperature ratios $\tau = T_{Si}/T_{Se}$ at the source. Simulation length L is $22\lambda_D$ for $\tau = 0.1$ and 1 and is $15\lambda_D$ for $\tau = 10$. Also indicated are minimum ion drift velocity at the collector sheath entrance as predicted by Stangeby[7] where $C_S/V_{ti} = (1 + 1/\tau)^{1/2}$. Drift velocities are normalized by the ion thermal velocity V_{ti} at the source.

IV. COMPARISON OF THEORETICAL AND SIMULATION RESULTS

Simulation values of ψ_P and ψ_C measured at $x = 0.5L$ and L coincide exactly with the values predicted using the simultaneous solution of Eqs. (19) and (20). Although two common solutions to Eqs. (19) and (20) do exist, as shown in Fig. 2, the simulated plasma chooses only the solution with $\psi_P \neq 0$. These measured simulation values of ψ_P and ψ_C, displayed in Fig. 3(a), are generated from four runs using $\mu = 1/40$ with $\tau = 0.1$, 1, and 10 and using $\mu = 1/100$ with $\tau = 1$. The bars on these data points indicate the small amplitude of oscillation of potential which diminishes as the number of simulation particles used per λ_D is increased.

The existence of a self-consistent, time-independent solution does not necessarily imply a temporally stable solution, as seen above. Burger[14] has observed in the particle simulation of an ion rich thermionic convertor that the plasma potential profile fluctuates between the self-consistent solution and a temporary "static" solution. He notes that the transition time between potential configurations is comparable to the ionic transit time of the convertor. In our simulation with a computation time that is six times an ionic transit time, the plasma potential profile evolves to only one configuration.

The spatial profiles derived analytically for all three values of τ fit very well on the profiles generated by simulation for the density, drift velocity, temperature, kinetic energy flux, and heat flux of both species. Recall that these moments (derived earlier in Eqs. (5), (9)–(12), and (14)–(19)) depend on the potential ψ. To illustrate this good fit, the theoretical profiles for temperature are plotted on the simulation results in Fig. 5(g). These theoretical temperatures are calculated with the potential profile in Fig. 5(c). This choice is justified because ψ_P and ψ_C obtained from simulation agree with theory.

An interesting question might be, how accurate is the electron density N_B obtained from using a Boltzmann factor? The answer is that N_B, as calculated from simulation values for ψ substituted into Eq. (13), yields a good approximation for $\mu\tau \ll 1$ except within the collector sheath. When dividing Eq. (13) by Eq. (12), one finds that

$$N_B(\psi)/N_e(\psi) = 2\Big[1 + \mathrm{erf}(\psi - \psi_C)^{1/2}\Big]^{-1}.$$

This expression shows that as $\psi(x) \to \psi_C$ then $N_B \to 2N_e$. For $x < L$ the Boltzmann approximation assumes a full-Maxwellian velocity distribution. At $x = L$, $f_e(\psi_C, v)$ suddenly becomes half-Maxwellian (The collector absorbs all electrons and emits none.) Thus electron density at the collector is half that predicted with a Boltzmann factor so that $N_B(\psi_C)/2 = N_e(\psi_C)$. With our kinetic evaluation, the electrons evolve gradually from nearly full-Maxwellian to half-Maxwellian as they pass through the collector sheath to the collector surface.

V. COMPARISON OF OUR THEORY TO PREVIOUS ANALYSES

A. Cold ions

Agreement also can be shown between our results for cool ions ($\tau = 0.1$) and models with cold ions $\tau = 0$. For a cold ion, warm electron plasma, Tonks and Langmuir[1] found that potential at the edge of the neutral region ($\nabla^2\psi \approx 0$) occurs at $\psi_1 = -0.854$. Indicated on Fig. 3(b), their value for ψ_1, which is independent of μ, occurs in the limit for the plasma neutrality approximation and when the electric field, located between the neutral and the collector sheath region, goes to infinity. For $M/m = 1836$ and $\tau = 0.1$, our theory shows that $\psi_P = -0.850$, as plotted in Fig. 3(b). Hence, our results agree in the limits of large mass ratio and of cold ions.

The minimum ion energy at the sheath edge, as used by three other authors, is compared in Table I to our analytical results for the second velocity moment

(kinetic energy) and the square of the first velocity moment (drift energy) at ψ_P and ψ_C for a hydrogen plasma ($\mu=1/1836$). The first comparison in Table I shows the Bohm criterion [4] for minimum kinetic energy of cold ions at the sheath edge. This criterion, which can be written in normalized units as

$$\langle V_i^2 \rangle V_{ti}^{-2} \geq \tau^{-1},$$

compares the best among the other authors to our results with $\tau=0.1$, 1, and 10 not only for $\langle V_i^2 \rangle$ but also for $\langle V_i \rangle$. Note that although this criterion describes our results, the equality relation does not predict the ion kinetic energy at the edge of the collector sheath.

B. Various temperature ratios

We find some differences when a broad range of τ is considered for analyses such as those of Stangeby[7], Chodura[8,9], and Bissell and Johnson[10] who use the generalized Bohm criterion of Harrison and Thompson[5]. (Refer to remarks in Sec. I B, regarding the limit of validity of the generalized Bohm criterion.)

Stangeby[7] requires that ions enter the sheath region, where $N_i \approx N_e$, with a drift velocity $\langle V_i \rangle$ of at least the ion acoustic velocity C_S using $C_S/V_{ti}=(1+1/\tau)^{1/2}$; these limits are marked in Fig. 7. For $\mu=1/40$, this limit is achieved for $|\psi|<|\psi_P|$ when $\tau=0.1$ and 1; this value is never reached for $\tau=10$. However, for $\mu=1/1836$ in Table I, this minimum for $\langle V_i \rangle$ is attained before reaching the collector for all three temperature ratios. With this limit on $\langle V_i \rangle$, Stangeby obtains the potential drop ψ_F between the sheath edge and the collector expressed as: $\psi_F=(1/2)\ln(2\pi\mu(1+\tau))$. This equation is plotted in Fig. 3(a) along with our theoretical and simulation results. For large M/m, Stangeby's ψ_F compares with our $|\psi_C-\psi_P|$ to within 1.3% for $\tau=1$, $|\psi_F|$ falls short of $|\psi_C-\psi_P|$ by 10% for $\tau=0.1$, and $|\psi_F|$ exceeds $|\psi_C-\psi_P|$

by 12% for $\tau = 10$. Hence, Stangeby's expression roughly predicts potential change across the collector sheath but not the value of collector potential ψ_C.

Chodura[8] varies, via simulation, the ratio of emitted ion flux to electron flux until the potential profile decreases monotonically. With this method for $\mu = 1/1836$, Chodura obtains $\psi_F = -2.9$ for $\tau = 0$ (cold ions), and $\psi_F = -2.3$ for $\tau = 1$. The result for cold ions is 15% greater than ours for $\tau = 0.1$. For $\tau = 1$, the result is 9% less than ours. In a second paper, Chodura[9] requires that the ions enter the sheath region with a minimum drift velocity of C_S using $C_S/V_{ti} = (5/3 + 1/\tau)^{1/2}$, which is slightly larger than that of Stangeby's. (The 5/3 term is the specific heat ratio of ions with three degrees of freedom.) As shown in the third comparison in Table I, Chodura's lower limit for $\langle V_i \rangle$ is attained in our simulations within $x < L$ for $\tau = 0.1$ and 1 but is never reached for $\tau = 10$.

Chodura[9] also studies the mean ion kinetic energy $\langle W \rangle$ in three velocity directions at the collector. By definition this quantity is identical to our value for $Q_i(\psi_C)/F$. In three dimensions, motion in the transverse directions contribute $2\tau T_{Se}$ to $\langle W \rangle$. Expressed in one dimension, Chodura's results become $\langle W \rangle / T_{Se} = 4.2$ for $\tau = 1$ and 3.4 for $\tau = 0$ when $\mu = 1/1836$. From our analysis $\langle W \rangle / T_{Se} = \tau - \psi_C$ which is 3.9 for $\tau = 1$ and is 3.5 for $\tau = 0.1$. In summary, for $\tau = 1$, Chodura's prediction of $\langle V_i \rangle$ entering the sheath region leads to a higher value of $\langle W \rangle$.

Bissell and Johnson[10] use the generalized Bohm criterion as the boundary condition for their kinetic plasma equation. Plotting our values of $-\psi_P$ (for $\mu = 1/1836$) in Fig. 2 of their paper, we find that these fall below their values of potential $-\psi_1$ at the plasma-sheath boundary with the closest agreement at $\tau = 0.1$. (In fact, our values are slightly below their plot of the results of Emmert *et al.*[2] at $-\psi_1$.) In Fig. 6 of their paper at $\tau = 1$, $\psi_C = -3.2$; whereas our results indicate $\psi_C = -2.9$. Bissell and Johnson's method of solution results in an infinite electric

field at the plasma-sheath edge. From the potential profiles in our Fig. 6, one can see that $-\nabla\psi$ is always finite.

We find close agreement with Emmert *et al.*[2] except at low mass ratio with high τ in their model of a collisionless, finite ion temperature plasma. Analytically, they solve a plasma equation, tied to a plasma-sheath equation, by modeling the ions kinetically and the electrons with a Boltzmann factor. The edge of the quasi-neutral region where $\psi = -\psi_1(\tau)$ (independent of μ) can be derived from Eq. (33) of their paper. Hence we calculate that $\psi_1(0.1) = 0.766$; $\psi(1) = 0.404$; and $\psi(10) = 0.072$ which form the curve ψ_1 plotted in Fig. 3(b). Referring to the general potential profile in Fig. 1, for each case one expects that $-\psi_1$, the edge of the quasi-neutral region, should be slightly larger than our $-\psi_P$, the center of the neutral region. In Fig. 3(b), this trend occurs for all but the region near $\tau = 0.1$. Perhaps when the potential curvature, $\nabla^2\psi \approx 0$, in the source sheath is sufficiently large, (as seen in Fig. 6 with $\tau = 1$) their quasi-neutral assumption may not be accurate as $\psi \to \psi_1$.

Emmert *et al.* also show that the potential drop from the neutral region to ψ_1 occurs only across the distributed source. Similarly, in our model with a planar source, the drop to ψ_P occurs over approximately $4\lambda_D$ which is a typical distance over which the plasma can become neutral. In addition, they discover from their analysis that the width of the distributed source has no effect on the value of ψ_C. Substituting ψ_1 into their Eq. (35) determines ψ_C for each τ; their values are plotted in our Fig. 3(a). Their assumption of Boltzmann electrons causes the greatest difference in results for $\mu < 1/400$ with $\tau = 10$. For the other values of τ (0.1 and 1), we have excellent agreement among the theory of Emmert *et al.*, our theory, and simulation for low mass ratio. For $\mu = 1/1836$, we differ from their results at most by 4% for reasons as yet unknown.

In the final week of writing this document, a discussion[24] with Emmert revealed that the basic difference between the models of Emmert *et al.*[2] and Bissel and Johnson[10] is in the shape of the ion source function. Bissel and Johnson use a source function with the Maxwellian shape of $\exp(-\beta v^2)$ so that the resultant ion distribution function is strongly peaked near zero velocity. Emmert *et al.* use a source function of the form $v\exp(-\beta v^2)$ which generates a Maxwellian ion distribution. The Maxwellian source function requires a greater ψ_1 to accelerate the greater population of low energy ions. The source utilized in our theory and simulation produces half-Maxwellian source ions, hence, our results for ψ_P are closer to ψ_1 from Emmert *et al.* If our simulation were modified to generate the ion distribution function of Bissel and Johnson, then we anticipate results similar to theirs. Hence, it seems that the resultant potential profile depends somewhat on the particular form of the ion distribution function specified at the source.

VI. CONCLUSIONS

We have presented analysis and simulation determining critical potential values for a half-Maxwellian source of ions and electrons which flow to an electrically floating collector. This analysis is verified over a specified range of $(mT_{Si})/(MT_{Se})$ from 1 to approximately 10^{-5}. Density, drift velocity, temperature, kinetic energy flux, and heat flux are derived at values of potential at the collector and across the source sheath. For all of the above values, excellent agreement exists between our electrostatic particle simulation and the fully kinetic model for (τ, μ) at $(10, 1/40)$, $(1, 1/40)$, $(1, 1/100)$, and $(0.1, 1/40)$. Previous studies, which assume a minimum ion drift velocity entering the collector sheath region, model roughly only the potential drop across the collector sheath, i.e. $\psi_C - \psi_P$. For the largest range of mass and temperature ratios, we encounter the closest agreement in ψ_C with the model of Emmert *et al.* However, even this model, which uses Boltzmann electrons, breaks

down as $\mu\tau \rightarrow 1$. (Experimental plasmas composed of heavy SF_6^--Ba^+ ions with $\mu \approx 1$ do exist.) Consequently our model is the nearest to first principles of the referenced works on collector sheaths in self-consistently modeling the dynamic and kinetic behavior of the electrons and ions in the non-neutral, non-Maxwellian region between a Maxwellian plasma source and collector.

Acknowledgments

We thank Dr. S. Kuhn for his persistence and guidance in persuading us to check simulation with his classic Q-machine model. Discussions with W. S. Lawson on proper modeling are gratefully recognized. This research was sponsored by the U. S. Department of Energy under Contract DE-FG03-86ER53220.

References

[1]L. Tonks and I. Langmuir, Phys. Rev., **34**, 876 (1929).

[2]G. A. Emmert, R. M. Wieland, A. T. Mense, and J. N. Davidson, Phys. Fluids, **23**, 803 (1980).

[3]D. A. Dunn, *Models of Particles and Moving Media*, (McGraw-Hill, New York, 1971), Chapter 6.

[4]D. Bohm, in *Characteristics of Electrical Discharges in Magnetic Fields*, edited by A. Guthrie and R. K. Wakerling (McGraw-Hill, New York, 1949).

[5]E. R. Harrison and W. B. Thompson, Proc. Phys. Soc., **74**, 145 (1959).

[6]L. S. Hall, Proc. Phys. Soc., **80**, 309 (1962).

[7]P. C. Stangeby, Phys. Fluids., **27**, 682 (1984).

[8]R. Chodura, Phys. Fluids, **25**, 1628 (1982).

[9]R. Chodura, J. Nucl. Mater., **111–112**, 420 (1982).

[10]R. C. Bissell and P. C. Johnson, Phys. Fluids, **30**, 779 (1987).

[11]S. Kuhn, Plasma Physics, **23**, 881 (1981).

[12]P. Auer, J. Appl. Phys., **31**, 2096 (1960).

[13]R. G. McIntyre, Proc. IEEE, **51**, 760 (1963).

[14]R. G. McIntyre, J. Appl. Phys., **33**, 2485 (1962).

[15]P. Burger, J. Appl. Phys., **36**, 1938 (1965).

[16]W. Ott, Z. Naturf., **22A**, 1057 (1967).

[17]N. Rynn, Phys. Fluids, **9**, 165 (1966).

[18]D. Nicholson, *Introduction to Plasma Theory*, (John Wiley and Sons, New York, 1983), Chapter 6.

[19]I. P. Shkarofsky, T. W. Johnston, and M. P. Bachynski, *The Particle Kinetics of Plasmas*, (Addison-Wesley, Reading, Massachusetts, 1966) Chapter 2.

[20]S. Kuhn, private conversation, Innsbruck, Austria, September 24, 1987.

[21]C. K. Birdsall and A. B. Langdon, *Plasma Physics via Computer Simulation*, (McGraw-Hill, New York, 1985).

[22]W. S. Lawson, "PDW1 User's Manual", Memo No. UCB/ERL M84/37, Electronics Research Laboratory, University of California, Berkeley, California (1984).

[23]D. Gabor, E. Ash, and D. Dracott, Nature, **176**, 916 (1955).

[24]Plasma Theory and Simulation Group meeting, EECS Dept., University of California, Berkeley, California, October 16, 1987.

Variable List

Symbol	Name
ϕ	Electrostatic potential
ϕ_P	Source sheath potential drop
ϕ_C	Collector potential
x	Spatial position
v	Velocity
M	Ion mass
$T_{S\alpha}$	Source temperature
$\langle V_M^n \rangle$	n^{th} velocity moment
C_S	Ion sound speed
α	Ion/electron emitted density ratio
m	Electron mass
μ	Electron/ion mass ratio
τ	Ion/electron source temperature ratio
L	System length
f_α	Velocity distribution function
E	Electric field
ρ	Net charge density
$V_{M\alpha}$	Cut-off velocity
$N_{S\alpha}$	Source density

ψ	Normalized potential
N_α	Particle density
F_α	Particle flux
T_α	Temperature
Q_α	Kinetic energy flux
H_α	Heat flux
F	Reference particle flux
N_B	Boltzmann electron density
$V_{t\alpha}$	Source thermal velocity
δ_t	Total energy transmission factor

The subscript α refers to ions i or electrons e.

The above is a list of only frequently referenced variables.